Field-induced Berry connection and anomalous planar Hall effect in tilted Weyl semimetals

YuanDong Wang [1,2] Zhen-Gang Zhu [1,2,3,*] and Gang Su [2,3,4,†]

[1]*School of Electronic, Electrical and Communication Engineering, University of Chinese Academy of Sciences, Beijing 100049, China*
[2]*School of Physical Sciences, University of Chinese Academy of Sciences, Beijing 100049, China*
[3]*CAS Center for Excellence in Topological Quantum Computation, University of Chinese Academy of Sciences, Beijing 100049, China*
[4]*Kavli Institute for Theoretical Sciences, University of Chinese Academy of Sciences, Beijing 100190, China*

(Received 16 December 2022; accepted 28 September 2023; published 16 November 2023)

We propose the linear and nonlinear *anomalous* planar Hall effect (APHE) in tilted Weyl semimetals in the presence of an in-plane magnetic and electric field, where the field-induced Berry connection plays a key role. The conductivity of linear APHE is ascribed to the quantum metric and is antisymmetric in nature, distinct from the well-known chiral anomaly induced PHE arising from the Berry curvature. Using a tilting vector to describe the model, we demonstrate the constrains on the linear and nonlinear APHE by the tilting directions. The linear APHE is intrinsic that is determined by the topological properties of energy bands, whereas the nonlinear APHE is extrinsic. The predicted linear and nonlinear APHE are inherently different from others and may shed light on a deeper understanding on transport nature of the tilted Weyl semimetals.

DOI: 10.1103/PhysRevResearch.5.043156

I. INTRODUCTION

Three-dimensional topological Weyl semimetals (WSMs), a new state of quantum matter with gapless spectrum at bulk nodal points and spin nondegenerate open Fermi arc states on the surface, has attracted much recent interest [1–8]. The Weyl monopoles hosted by topological semimetals, as sources or sinks of the Berry curvature may lead to a number of nontrivial transport effects, including the anomalous Hall effect [1,9–12], in which a transverse charge current proportional to the Berry curvature is generated in response to a longitudinal electric field without external magnetic fields, the "chiral anomaly" [13–16] that breaks the chiral symmetry leading to the nonconservation of chiral charges, etc. Until now, the negative longitudinal magnetoresistance and the planar Hall effect (PHE) are the most remarkable phenomena induced by the chiral anomaly [17–22]. For the PHE, a net charge current $\boldsymbol{J} \propto (\boldsymbol{E}\cdot\boldsymbol{B})\boldsymbol{B}$ [23–26] can be induced due to chiral anomaly and nonconservation of density of electrons at an individual node when the magnetic field and the electric field are nonorthogonal (i.e., $\boldsymbol{E}\cdot\boldsymbol{B}\neq 0$) [13]. Notably, the conductivity tensor for the PHE is symmetric in nature, and it does not contribute to the genuine (dissipationless) Hall conductivity which is required to be antisymmetric with $\sigma_{\mathcal{H}}^{yx}=-\sigma_{\mathcal{H}}^{xy}$ [27,28].

The Berry curvature can be recognized as the imaginary part of a quantum geometric tensor [29,30], whereas the real part of this tensor is another important geometric quantity called quantum metric [31], which allows us to measure the distance between quantum states. The concept of the quantum metric was well applied in quantum information theory [32–36], and it begins to attract attention in condensed-matter physics [37–41]. Recently, the quantum metric is found to have relationship with field-induced Berry connection (FBC) [42,43] by invoking a generalized semiclassical theory. Therefore, it is quite imperative to know whether a measurable effect can exist to reflect the character of the quantum metric.

Different to the ohmic PHE from chiral anomaly, recently it has been proposed that a genuine Hall effect with antisymmetric conductivity tensor is generated via the spin-Zeeman coupling, known as anomalous planar Hall effect (APHE) [27], or alternatively, referred as "in-plane Hall effect" [44,45]. In this paper, we propose an intrinsic linear and extrinsic nonlinear APHE inherent to the quantum metric linked via FBC. This may provide a direct method unveiling the profound connection between transport in condensed matters and the quantum metric. Since the linear effect should be dominant in the transport when the linear and nonlinear effects occur simultaneously, the proposed intrinsic linear APHE is crucial. Remarkably, we find that in a two-band tilted WSM model, the APHE is generated via the magnetic-field-induced Berry connection (B-FBC) that results in an antisymmetric Hall current [46], in contrast with the symmetric Hall (ohmic) current such as transverse Drude current and the PHE induced by chiral anomaly. The nonlinear APHE proposed here is extrinsic that differs from others. It is found that both of E-FBC and B-FBC contribute to the nonlinear APHE, with the B-FBC (E-FBC) conductivity being an antisymmetric (asymmetric) third-rank tensor. Moreover, we point out the case in which the linear APHE disappears whereas the nonlinear

*zgzhu@ucas.ac.cn
†gsu@ucas.ac.cn

APHE is dominant, which is also enlightening to topological nonlinearity.

II. FIELD-INDUCED BERRY CONNECTION AND THE CORRESPONDING CURRENT

We start from the Berry curvature of the nth band, which is defined by

$$\boldsymbol{\Omega}_n(\boldsymbol{k}) = \nabla_{\boldsymbol{k}} \times \boldsymbol{\mathcal{A}}_n(\boldsymbol{k}), \tag{1}$$

where $\boldsymbol{\mathcal{A}}_n(\boldsymbol{k}) = i\langle u_{n\boldsymbol{k}}|\nabla_{\boldsymbol{k}}|u_{n\boldsymbol{k}}\rangle$ is the intraband Berry connection with $|u_{n\boldsymbol{k}}\rangle$ being the periodic part of the nth Bloch state. In the presence of electric field $\boldsymbol{E}$ and magnetic field $\boldsymbol{B}$, the Berry connection acquires a gauge-invariant correction besides $\boldsymbol{\mathcal{A}}_n(\boldsymbol{k})$, which is written as

$$\boldsymbol{\mathcal{A}}'_n = \boldsymbol{\mathcal{A}}'_n(E) + \boldsymbol{\mathcal{A}}'_n(B). \tag{2}$$

As a result, the Berry curvature is extended to $\tilde{\boldsymbol{\Omega}}_n = \boldsymbol{\Omega}_n + \boldsymbol{\Omega}'_n$ with $\boldsymbol{\Omega}'_n = \nabla \times \boldsymbol{\mathcal{A}}'_n$. The E-FBC can be written as $\boldsymbol{\mathcal{A}}'_n(E) = \overleftrightarrow{\boldsymbol{G}}_n \boldsymbol{E}$, where the double arrow indicates the second-rank tensor, which is given by [42,47,48]

$$(\overleftrightarrow{\boldsymbol{G}}_n)^{\alpha\beta} = G_n^{\alpha\beta} = 2\sum_{m\neq n} \frac{\mathrm{Re}\left[\mathcal{A}^{\alpha}_{nm}\mathcal{A}^{\beta}_{mn}\right]}{\varepsilon_n - \varepsilon_m}, \tag{3}$$

where $\boldsymbol{\mathcal{A}}_{nm} = i\langle u_{n\boldsymbol{k}}|\nabla_{\boldsymbol{k}}|u_{m\boldsymbol{k}}\rangle$ is the interband Berry connection, and ε_n is the unperturbed band energy where for simplicity the modification caused by the orbital magnetic moment is not considered. The magnetic-field counterpart is $\boldsymbol{\mathcal{A}}'_n(B) = \overleftrightarrow{\boldsymbol{F}}_n \boldsymbol{B}$ [42,47] with

$$F_n^{\alpha\beta} = \mathrm{Im}\sum_{m,p\neq n} \frac{\mathcal{A}^{\alpha}_{nm}\epsilon^{\beta\gamma\delta}\left[(\varepsilon_p - \varepsilon_m)\mathcal{A}^{\gamma}_{mp} + iv_n^{\gamma}\delta_{mp}\right]\mathcal{A}^{\delta}_{pn}}{\varepsilon_n - \varepsilon_m}, \tag{4}$$

in which $\boldsymbol{v}_n = (1/\hbar)\partial\varepsilon_n/\partial\boldsymbol{k}$ is the group velocity. Note that the Berry connection involves a sum over all pairs of bands with $g^{\alpha\beta}_{nm} = \mathrm{Re}[\mathcal{A}^{\alpha}_{nm}\mathcal{A}^{\beta}_{mn}]$, which is recognized as the quantum metric for two-band systems [49,50].

The semiclassical equations of motion read [51,52] (for brevity the sum of the band index is implied)

$$D(\boldsymbol{B},\tilde{\boldsymbol{\Omega}})\dot{\boldsymbol{r}} = \left[\boldsymbol{v}_{\boldsymbol{k}} + \frac{e}{\hbar}\boldsymbol{E}\times\tilde{\boldsymbol{\Omega}}_{\boldsymbol{k}} + \frac{e}{\hbar}(\boldsymbol{v}_{\boldsymbol{k}}\cdot\tilde{\boldsymbol{\Omega}}_{\boldsymbol{k}})\boldsymbol{B}\right], \tag{5}$$

$$D(\boldsymbol{B},\tilde{\boldsymbol{\Omega}})\dot{\boldsymbol{k}} = \left[-\frac{e}{\hbar}\boldsymbol{E} - \frac{e}{\hbar}\boldsymbol{v}_{\boldsymbol{k}}\times\boldsymbol{B} - \frac{e^2}{\hbar^2}(\boldsymbol{E}\cdot\boldsymbol{B})\tilde{\boldsymbol{\Omega}}_{\boldsymbol{k}}\right], \tag{6}$$

where $D(\boldsymbol{B},\tilde{\boldsymbol{\Omega}}) = (1 + e\boldsymbol{B}\cdot\tilde{\boldsymbol{\Omega}}/\hbar)$ is the phase volume factor [51,53] revealed in the presence of nonzero Berry curvature $\tilde{\boldsymbol{\Omega}}$ and magnetic field $\boldsymbol{B}$, which is written as D in the following for a shorthand notation. e is the (positive) elementary charge. The anomalous velocity includes a magnetic-field-dependent term, which indicates that the electrons move along the magnetic-field direction for one Weyl cone and along the opposite direction for the cone with the opposite chirality. Noting that in Eqs. (5) and (6), the correction of the orbital magnetic moment (OMM) to the band energy is included, which is written as $\tilde{\varepsilon}_{\boldsymbol{k}} = \varepsilon_{\boldsymbol{k}} - \boldsymbol{m}_{\boldsymbol{k}}\cdot\boldsymbol{B}$ with the OMM given by

$$\boldsymbol{m}_{\boldsymbol{k}} = -i\frac{e}{2\hbar}\langle\nabla_{\boldsymbol{k}}u_{\boldsymbol{k}}|\times(\hat{H} - \varepsilon_{\boldsymbol{k}})|\nabla_{\boldsymbol{k}}u_{\boldsymbol{k}}\rangle. \tag{7}$$

In the semiclassical framework, the total current response for a uniform system can be expressed as

$$\boldsymbol{J} = -e\int [d\boldsymbol{k}]D\dot{\boldsymbol{r}}f(\tilde{\varepsilon}_{\boldsymbol{k}}), \tag{8}$$

where $[d\boldsymbol{k}]$ is a shorthand notation for $d\boldsymbol{k}/(2\pi)^d$, $f(\tilde{\varepsilon}_{\boldsymbol{k}})$ is the single-particle distribution function. To calculate the current density, we use the homogeneous steady-state Boltzmann equation within the relaxation-time approximation to solve the distribution function:

$$\dot{\boldsymbol{k}}\cdot\nabla_{\boldsymbol{k}}f = \frac{f_0 - f}{\tau}, \tag{9}$$

where f_0 is the equilibrium Fermi-Dirac distribution, and τ is the transport relaxation time. To obtain the general expressions for the nonlinear currents, Eq. (9) is solved by expanding the distribution function up to the second order in $\boldsymbol{E}$ as $f = f_0 + f_1 + f_2$, where

$$f_1 = \frac{\tau}{D}\left[e\boldsymbol{E}\cdot\boldsymbol{v}_{\boldsymbol{k}} + \frac{e^2}{\hbar}(\boldsymbol{E}\cdot\boldsymbol{B})(\boldsymbol{\Omega}_{\boldsymbol{k}}\cdot\boldsymbol{v}_{\boldsymbol{k}})\right]\frac{\partial f_0}{\partial\varepsilon_{\boldsymbol{k}}}, \tag{10}$$

$$f_2 = \frac{\tau}{D}\left[e\boldsymbol{E}\cdot\boldsymbol{v}_{\boldsymbol{k}} + \frac{e^2}{\hbar}(\boldsymbol{E}\cdot\boldsymbol{B})(\boldsymbol{\Omega}_{\boldsymbol{k}}\cdot\boldsymbol{v}_{\boldsymbol{k}})\right]\frac{\partial f_1}{\partial\varepsilon_{\boldsymbol{k}}} + \frac{\tau}{D}\left[\frac{e^2}{\hbar}(\boldsymbol{E}\cdot\boldsymbol{B})(\nabla\times(\overleftrightarrow{\boldsymbol{G}}\boldsymbol{E})\cdot\boldsymbol{v}_{\boldsymbol{k}})\right]\frac{\partial f_0}{\partial\varepsilon_{\boldsymbol{k}}}. \tag{11}$$

III. THE INTRINSIC LINEAR APHE DUE TO FBC

First, we focus on the in-plane (the magnetic field, electric field, and the current coplanar) linear current scales with the order of $O(EB)$. Noting that OMM contributes to the current in order of $O(EB)$, which is given as $\boldsymbol{J}^{(1)}_{\mathrm{OMM}} = \frac{e^2}{\hbar}\boldsymbol{E}\times\int[d\boldsymbol{k}]\boldsymbol{\Omega}_{\boldsymbol{k}}(\boldsymbol{m}_{\boldsymbol{k}}\cdot\boldsymbol{B})\frac{\partial f_0}{\partial\varepsilon_{\boldsymbol{k}}}$ [54]. In the following, we show that $\boldsymbol{J}^{(1)}_{\mathrm{OMM}}$ will not contribute to the in-plane current in WSMs when $\boldsymbol{B}$ lies in the transport plane, so we ignore it in the study of the in-plane current.

Substituting the first-order distribution function Eq. (10) into Eq. (8), the linear in-plane current up to the order $O(EB)$ in the presence of external fields is obtained as

$$\boldsymbol{J}^{(1)} = \boldsymbol{J}^{(1)}_{\mathrm{AB}} + \boldsymbol{J}^{(1)}_{\mathrm{CA}} + \boldsymbol{J}^{(1)}_{\mathrm{FBC}}. \tag{12}$$

The first term is attributed to the anomalous velocity due to magnetic field (the meaning of index "AB"), which is given by

$$\boldsymbol{J}^{(1)}_{\mathrm{AB}} = -\frac{e^3\tau}{\hbar}\int[d\boldsymbol{k}]\frac{\partial f_0}{\partial\varepsilon_{\boldsymbol{k}}}(\boldsymbol{v}_{\boldsymbol{k}}\cdot\boldsymbol{\Omega}_{\boldsymbol{k}})(\boldsymbol{E}\cdot\boldsymbol{v}_{\boldsymbol{k}})\boldsymbol{B}. \tag{13}$$

This term is generally nonzero for a single cone. When the two cones are tilted in opposite directions, the distributions in two cones shift along the opposite directions due to the modified $\boldsymbol{v}_{\boldsymbol{k}}$, resulting in a finite $\boldsymbol{J}^{(1)}_{\mathrm{AB}}$ [55].

The second term in Eq. (12) stems from the effective chiral chemical potential [the third term in Eq. (6)] due to the chiral anomaly (for the index "CA"), which is

$$\boldsymbol{J}^{(1)}_{\mathrm{CA}} = -\frac{e^3\tau}{\hbar}\int[d\boldsymbol{k}]\frac{\partial f_0}{\partial\varepsilon_{\boldsymbol{k}}}(\boldsymbol{E}\cdot\boldsymbol{B})(\boldsymbol{\Omega}_{\boldsymbol{k}}\cdot\boldsymbol{v}_{\boldsymbol{k}})\boldsymbol{v}_{\boldsymbol{k}}. \tag{14}$$

In the absence of the tilting, for the two-cone model of the WSMs with time-reversal symmetry, the contribution of this

term is zero [20,55]. $\boldsymbol{J}^{(1)}_{\rm AB}$ and $\boldsymbol{J}^{(1)}_{\rm CA}$ are all responsible for the planar Hall effect, where the Hall current, the electric and magnetic fields are all coplanar.

With considering the FBC effect, we find a different kind of APHE, which is given as

$$\boldsymbol{J}^{(1)}_{\rm FBC} = -\frac{e^2}{\hbar}\int [d\boldsymbol{k}] f_0 \{\boldsymbol{v}_{\boldsymbol{k}} \cdot [\nabla \times (\overleftrightarrow{\boldsymbol{G}}\boldsymbol{E})]\boldsymbol{B} + \boldsymbol{E}[\nabla \times (\overleftrightarrow{\boldsymbol{F}}\boldsymbol{B})]\}. \tag{15}$$

Here the first term is the E-FBC component and the second term is the B-FBC component. The corresponding linear anomalous planar Hall conductivity (APHC) is given by the sum $\sigma^{\alpha\beta}_{\rm FBC} = \sigma^{\alpha\beta}_{\text{E-FBC}} + \sigma^{\alpha\beta}_{\text{B-FBC}}$.

We first investigate the E-FBC component, which is given by

$$\sigma^{\alpha\beta}_{\text{E-FBC}} = -\frac{e^2}{\hbar}\sum_n \int [d\boldsymbol{k}] f^n_0 v^\gamma_n \epsilon^{\gamma\delta\zeta}\partial^\zeta G^{\delta\beta}_n B^\alpha, \tag{16}$$

where the sum over the repeated Greek indices is implicit. When f_0 attains a superscript of n, it means the equilibrium Fermi-Dirac distribution for the nth band. From Eq. (16), it is straightforward to see that the conductivity tensor of the E-FBC contribution is asymmetric by exchanging the indices α and β. According to Ref. [46], it can be separated into a symmetric (ohmic) component and an antisymmetric (genuine Hall) component.

The B-FBC contribution can be obtained by

$$\sigma^{\alpha\beta}_{\text{B-FBC}} = -\frac{e^2}{\hbar}\sum_n \int [d\boldsymbol{k}] f^n_0 \epsilon^{\beta\gamma\alpha}\epsilon^{\delta\zeta\gamma}\partial^\delta F^{\zeta\eta}_n B^\eta. \tag{17}$$

Noting that $\sigma^{\alpha\beta}_{\text{B-FBC}} = -\sigma^{\beta\alpha}_{\text{B-FBC}}$, it manifests as a genuine Hall current. A few general remarks on the FBC-induced linear APHE are in order. First, $\sigma^{\alpha\beta}_{\rm FBC}$ is allowed by time-reversal symmetry. For linear APHE, the whole set of the external field EB, as well as the current, is odd for both of $\mathcal{T}$ and $\mathcal{P}$ symmetry, so nonzero response is allowed in either WSMs with $\mathcal{T}$ symmetry or $\mathcal{P}$ symmetry. The $\mathcal{T}$ ($\mathcal{P}$) symmetry leads to $\boldsymbol{\mathcal{A}}_{nm}(\boldsymbol{k}) = \boldsymbol{\mathcal{A}}_{mn}(-\boldsymbol{k})$ [$\boldsymbol{\mathcal{A}}_{nm}(\boldsymbol{k}) = \boldsymbol{\mathcal{A}}_{mn}(-\boldsymbol{k})$], and it can be verified that $G^{\alpha\beta}_n(\boldsymbol{k}) = G^{\alpha\beta}_n(-\boldsymbol{k})$ and $F^{\alpha\beta}_n(\boldsymbol{k}) = -F^{\alpha\beta}_n(-\boldsymbol{k})$ for either $\mathcal{T}$ or $\mathcal{P}$ symmetry. Thus, $\sigma^{\alpha\beta}_{\rm FBC}$ is even for either $\mathcal{T}$ or $\mathcal{P}$ symmetry. However, considering that both of $\boldsymbol{J}_{\rm AB}$ and $\boldsymbol{J}_{\rm CA}$ are proportional to τEB that is $\mathcal{T}$ even, it results in vanishing of $\boldsymbol{J}_{\rm AB}$ and $\boldsymbol{J}_{\rm CA}$ in $\mathcal{T}$-symmetric systems leaving the $\boldsymbol{J}_{\rm FBC}$ as the dominant contribution irrespective of the tilting direction. Second, $\boldsymbol{J}^{(1)}_{\rm FBC}$ is independent of the relaxation time τ, manifesting it as an intrinsic effect determined solely by the band structure of the materials. Third, for $\sigma^{xx}_{\text{B-FBC}}$ the longitudinal component is forbidden, leaving it as a pure Hall current. While for $\sigma^{\alpha\beta}_{\text{E-FBC}}$ both of the longitudinal and Hall components are allowed.

IV. FBC-INDUCED LINEAR APHE IN WSMS

With the help of the general expressions of the APHE arising from FBC in Eqs. (16) and (17), we are now in the position to investigate the APHE with FBC in WSMs. The low-energy effective Hamiltonian describing the WSMs can be written as [8]

$$H = v_{\rm F}(s\boldsymbol{k}\cdot\boldsymbol{\sigma} + \boldsymbol{R}_s\cdot\boldsymbol{k}\sigma_0), \tag{18}$$

where $s = \pm 1$ specify the chiralities of the Weyl nodes, σ_0 is the 2×2 identity matrix, $\boldsymbol{\sigma} = (\sigma^x, \sigma^y, \sigma^z)$ are the Pauli matrices, v_F is the Fermi velocity and $\boldsymbol{R}_s = (R^x_s, R^y_s, R^z_s)$ is the tilting vector of the Weyl cone. The WSM Hamiltonian (without tilting) can be realized by either breaking time-reversal symmetry $\mathcal{T}$ or inversion symmetry $\mathcal{P}$. Note that the tilting term breaks $\mathcal{T}$ symmetry by itself.[1] For a specific tilting when the pair of Weyl cones are tilted in same direction, it also breaks the $\mathcal{P}$ symmetry. As a consequence, the Weyl nodes of Hamiltonian Eq. (18) can be obtained by breaking either $\mathcal{T}$ or $\mathcal{P}$ symmetry. With the Hamiltonian Eq. (18), the energy dispersion for a Weyl cone of chirality s is derived as

$$\varepsilon_{s,\pm} = v_{\rm F}(\boldsymbol{R}_s\cdot\boldsymbol{k} \pm k), \tag{19}$$

where the $+$ ($-$) sign corresponds to the conduction (valence) band and $k = |\boldsymbol{k}|$. The group velocity is $\boldsymbol{v}_s = v_F(\frac{k^x}{k} + R^x_s, \frac{k^y}{k} + R^y_s, \frac{k^z}{k} + R^z_s)$.

Before proceeding further, we introduce the quantum metric which is closely related to the FBC in WSMs. The proper distance between quantum states can be defined as $dr^2 = Q^{\alpha\beta}k^\alpha k^\beta$, where $Q^{\alpha\beta} = \langle\partial^\alpha\psi|\partial^\beta\psi\rangle - \langle\partial^\alpha\psi|\psi\rangle\langle\psi|\partial^\beta\psi\rangle$ is the quantum geometric tensor [31,49,56–58]. Its imaginary part, $\text{Im}[Q^{\alpha\beta}] = \varepsilon^{\alpha\beta\gamma}\Omega^\gamma$, is the antisymmetric tensor Berry curvature, and its real part is the Fubini-Study quantum metric $g^{\alpha\beta}$, $\text{Re}[Q^{\alpha\beta}] = g^{\alpha\beta}$, which is the symmetric tensor. Specially, for the two band Hamiltonian, the products of Berry connections can be rewritten by the quantum metric. For example, the quantum metric tensor for the Weyl cone with chirality s of the valence band is written as $g^{\alpha\beta}_{s-} = \text{Re}[\mathcal{A}^\alpha_{s-+}\mathcal{A}^\beta_{s+-}]$, and we obtain

$$G^{\alpha\beta}_{s-} = 2g^{\alpha\beta}_{s-}/(\varepsilon_{s-} - \varepsilon_{s+}). \tag{20}$$

One observes that the quantum metric is directly related to the FBC. The Berry curvature and the OMM are given by $\boldsymbol{\Omega}^s_{\boldsymbol{k}} = -s(\pm\boldsymbol{k}/|\boldsymbol{k}|^3)$, $\boldsymbol{m}^s_{\boldsymbol{k}} = -sev_F(\pm\boldsymbol{k}/|\boldsymbol{k}|^3)$. It is seen that the Berry curvature and OMM are in parallel. As they are in the z direction, $\boldsymbol{J}^{(1)}_{\rm OMM}$ is zero for when $\boldsymbol{B}$ is in the transport plane. When they are also lying in the plane as $\boldsymbol{B}$, $\boldsymbol{J}^{(1)}_{\rm OMM}$ will not contribute to in-plane current.

To get analytical results, we restrict our discussion within the type-I WSMs, where we can only consider the conduction band when the chemical potential lies above the Weyl nodes, and we drop the band indices in the following.

Let us consider the situation that a pair of Weyl cones are tilted in the same direction, in which $\boldsymbol{J}^{(1)}_{\rm AB}$ and $\boldsymbol{J}^{(1)}_{\rm CA}$ vanish, and $\boldsymbol{J}^{(1)}_{\rm FBC}$ is dominated in the linear PHE. We suppose that the electric field is directed along the x axis, $\boldsymbol{E} = E\hat{x}$, and the magnetic field lies in the $x-y$ plane with an angle from the x axis is θ, i.e., $\boldsymbol{B} = B\cos\theta\hat{x} + B\sin\theta\hat{y}$. For the same tilting direction, $\boldsymbol{R}_s = \boldsymbol{R}$, and the APHC induced by the E-FBC is

[1] When we refer to the $\mathcal{T}$-breaking tilted WSM, we mean that it is $\mathcal{T}$ breaking even at zero tilt.

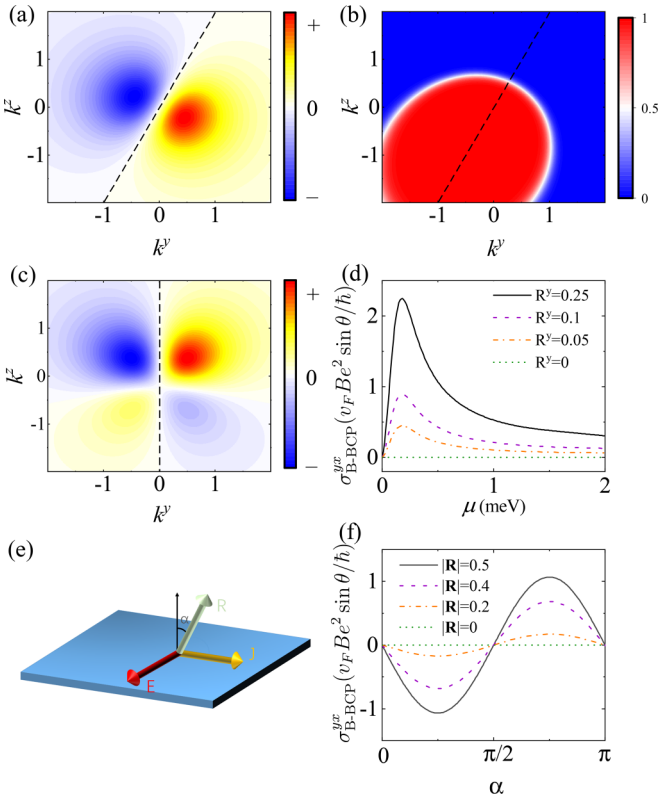

FIG. 1. (a) The integrand Γ^{yz} for $\sigma^{yx}_{\text{E-FBC}}$. (b) The equilibrium state distribution f_0. (c) The integrand $\mathcal{F}^{yxy}$ for $\sigma^{yx}_{\text{B-FBC}}$. For panels (a)–(c) the momentum plane is $k^x = 1$. (d) $\sigma^{yx}_{\text{B-FBC}}$ versus chemical potential μ for different values of R^y, R^x is set to zero and R^z is set to 0.5. In the calculation, we take $k_BT = 20$ meV. (e) Diagrammatic sketch for the tilting vector $\boldsymbol{R}$. (f) $\sigma^{yx}_{\text{B-FBC}}$ as a function of tilting angle α for different values of the magnitude of $\boldsymbol{R}$.

obtained as (see Appendix A)

$$\sigma^{yx}_{\text{E-FBC}} = -\frac{e^2}{\hbar}\int [d\boldsymbol{k}] f_0 \Gamma^{yz} v_{\text{F}} B \sin\theta, \tag{21}$$

where $\Gamma^{yz} = \frac{4}{k^5}(R^z k^y - R^y k^z)$. One may observe that there is an antisymmetry mirror line with the slope $k^y/k^z = R^y/R^z$ for Γ^{yx} in the $k^y - k^z$ plane, as shown in Fig. 1(a), with the tilting parameters $R^y = 0.25$ and $R^z = 0.5$. However, the equilibrium distribution function f_0 is symmetric with respect to the mirror line, which is depicted in Fig. 1(b). Combining f_0 and Γ^{yz}, it renders the cancellation of the integration in momentum space, leaving $\sigma^{yx}_{\text{E-FBC}}$ vanishes and thus we have $\sigma^{yx}_{\text{FBC}} = \sigma^{yx}_{\text{B-FBC}}$.

Now we investigate the linear APHE induced by the B-FBC. According to Eq. (15) and making use of the two-band nature of the WSMs Hamiltonian, the complex expression of the B-FBC equation (4) reduces to a simple form

$$F^{\alpha\beta}_{s-} = \text{Re}\frac{\epsilon^{\beta\gamma\delta} v^{\gamma}_{s-} \mathcal{A}^{\alpha}_{s-+} \mathcal{A}^{\delta}_{s+-}}{\varepsilon_{s-} - \varepsilon_{s+}} = \frac{\epsilon^{\beta\gamma\delta} v^{\gamma}_{s-} g^{\alpha\beta}_{s-}}{\varepsilon_{s-} - \varepsilon_{s+}}. \tag{22}$$

When both Weyl cones are tilted in the same direction, the linear APHE induced by B-FBC reads (see Appendix A)

$$\sigma^{yx}_{\text{B-FBC}} = \frac{e^2}{\hbar}\int [d\boldsymbol{k}] f_0 (\mathcal{F}^{yxy}\sin\theta + \mathcal{F}^{yxx}\cos\theta) v_{\text{F}} B, \tag{23}$$

where $\mathcal{F}^{\alpha\beta\gamma}_s = \partial^{\alpha} F^{\beta\gamma}_s - \partial^{\beta} F^{\alpha\gamma}_s$ and we have

$$\mathcal{F}^{yxy} = \frac{k^y(2k^z + kR^z)}{2k^6}, \quad \mathcal{F}^{yxx} = \frac{k^x(2k^z + kR^z)}{2k^6}. \tag{24}$$

A particular case is that R^z is zero. We thus notice that $\mathcal{F}^{yxy}$ and $\mathcal{F}^{yxx}$ are odd with respect to k^z; whereas f_0 is even, it leads to a vanishing $\sigma^{yx}_{\text{B-FBC}}$. In this case, the APHCs induced by E-FBC and B-FBC are both zero. Therefore a finite R^z is required for a nonvanishing $\sigma^{yx}_{\text{B-FBC}}$, namely, a perpendicular component of the tilting vector is required. Furthermore, $\sigma^{yx}_{\text{B-FBC}}$ vanishes if $R^y = R^x = 0$. This is because $\mathcal{F}^{yxy}$ ($\mathcal{F}^{yxx}$) is odd with respect to k^y (k^x), as shown in Fig. 1(c) (where the contour plot of $\mathcal{F}^{yxy}$ in the $k^y - k^z$ plane is shown). R^y (R^x) breaks the reflection symmetry about the k^y (k^x) axis for f_0, leading to a finite $\sigma^{yx}_{\text{B-FBC}}$. In Fig. 1(d) we plot $\sigma^{yx}_{\text{B-FBC}}$ as a function of the chemical potential μ for different values of R^y (R^x is set to zero). One observes that the magnitude of $\sigma^{yx}_{\text{B-FBC}}$ decreases for smaller R^y, as expected from symmetry analysis. It is worth noting that the dependence on the tilting directions for the APHE induced by FBC is very different from the chiral anomaly counterpart [on the order $O(EB)$], which vanishes when the nodes tilt along the same direction [55]. As a consequence, when the tilting of the two nodes is noncollinear, the two APHEs coexist (for more details see Appendix B). Noting that the APHE induced by FBC is antisymmetric with $\sigma^{yx}_{\text{FBC}} = -\sigma^{xy}_{\text{FBC}}$, while the PHE induced by chiral anomaly is symmetric with $\sigma^{yx}_{\text{CA}} = \sigma^{xy}_{\text{CA}}$. It serves as a character to distinguish these two PHEs in experiments.

To conclude, when both Weyl cones are tilted in the same direction, the APHE arising from FBC is finite if the angle α is not zero, nor $\pi/2$, as schematically illustrated in Fig. 1(e), and the dependence of the tilting angle α for $\sigma^{yx}_{\text{B-FBC}}$ is shown in Fig. 1(f). It differs significantly from the linear PHE induced by the chiral anomaly where the Weyl nodes tilt along opposite directions. Recently, an unconventional planar Hall effect was reported in the Weyl semimetal material $ZrTe_5$ [59] for which a remarkable discovery is the nonzero Hall conductivity when the in-plane magnetic field is parallel or perpendicular to the current, which is not included in previous theoretical and experimental studies (where such a conductivity disappears for the parallel case) but consistent with the planar Hall effect we propose here. We anticipate that this different kind of linear APHE can be observed in type-I WSMs such as TaAs [2,60] with strain-controlled tilting.

V. FBC-INDUCED NONLINEAR APHE IN WSMS

We already know that when the tilting vector lies along the normal to the transport plane, the linear FBC-induced APHE vanishes and the second-order response dominates. The nonlinear Hall effect in WSMs induced by the chiral anomaly as well as the Berry curvature dipole has been investigated in Refs. [61–65]. Here we show that the FBC can also induce a nonlinear APHE. Recently, an intrinsic nonlinear APHE has been proposed [66], where the effect of magnetic field plays a role via a magnetic-field-induced correction to the electric-field-induced correction of the Berry connection. For a comparison, we treat the effects of electric field and magnetic field on the same footing so that the proposed linear

TABLE I. List of constraints on the linear and second-order APHCs by the tilting directions of the Weyl nodes. The allowed (forbidden) APHCs are indicated by ✓ (×).

	$R^x = R^y = R^z = 0$	$R^z = 0$, R^x or $R^y \neq 0$	$R^z \neq 0$, $R^x = R^y = 0$	$R^z \neq 0$, R^x or $R^y \neq 0$
1st order	×	×	×	✓
2nd order	×	×	✓	✓

and nonlinear APHE are completely different from that in Ref. [66].

Combining Eqs. (10), (11), and (5), the second-order electric current induced by FBC is obtained as

$$\begin{aligned}\boldsymbol{J}^{(2)}_{\rm FBC} = -\frac{e^3\tau}{\hbar}\int [d\boldsymbol{k}]\{&[\nabla\times(\overleftrightarrow{\boldsymbol{G}}\,\boldsymbol{E})]\times(\boldsymbol{B}\times\boldsymbol{v}_{\boldsymbol{k}})(\boldsymbol{E}\cdot\boldsymbol{v}_{\boldsymbol{k}})\\ &+(\boldsymbol{E}\cdot\boldsymbol{B})\boldsymbol{v}_{\boldsymbol{k}}[\nabla\times(\overleftrightarrow{\boldsymbol{G}}\,\boldsymbol{E})]\cdot\boldsymbol{v}_{\boldsymbol{k}}\\ &+\boldsymbol{E}\times[\nabla\times(\overleftrightarrow{\boldsymbol{F}}\,\boldsymbol{B})]\boldsymbol{E}\cdot\boldsymbol{v}_{\boldsymbol{k}}\}\frac{\partial f_0}{\partial\varepsilon_{\boldsymbol{k}}},\end{aligned} \tag{25}$$

where the first two terms are contributed from the E-FBC, with a defined second-order APHC $\sigma^{\alpha\beta\gamma}_{\rm E\text{-}FBC}$:

$$\begin{aligned}\sigma^{\alpha\beta\gamma}_{\rm E\text{-}FBC} = -\frac{e^3\tau}{\hbar}\sum_n\int [d\boldsymbol{k}]\frac{\partial f_0}{\partial\varepsilon_{\boldsymbol{k}}}\epsilon^{\mu\nu\delta}\partial^\mu\\ \times G_n^{\nu\gamma}(\epsilon^{\delta\zeta\alpha}\epsilon^{\iota\kappa\zeta}v^\kappa v^\beta B^\iota + v^\alpha v^\delta B^\beta).\end{aligned} \tag{26}$$

It is seen that $\sigma^{\alpha\beta\gamma}_{\rm E\text{-}FBC}$ is a asymmetric three-rank tensor, and it can be separated into a symmetric and an antisymmetric component. The third term is the B-FBC contribution $\sigma^{\alpha\beta\gamma}_{\rm B\text{-}FBC}$:

$$\sigma^{\alpha\beta\gamma}_{\rm B\text{-}FBC} = -\frac{e^3\tau}{\hbar}\sum_n\int [d\boldsymbol{k}]\frac{\partial f_0}{\partial\varepsilon_{\boldsymbol{k}}}\epsilon^{\beta\delta\alpha}\epsilon^{\mu\nu\delta}B^\zeta v^\gamma\partial^\mu F_n^{v\zeta}. \tag{27}$$

One observes that $\sigma^{\alpha\beta\gamma}_{\rm B\text{-}FBC}$ is antisymmetric by exchanging first two indices, and it can be recognized as a genuine Hall current. The total second-order FBC-induced APHC is then $\sigma^{yxx}_{\rm FBC} = \sigma^{yxx}_{\rm E\text{-}FBC} + \sigma^{yxx}_{\rm B\text{-}FBC}$. For the nonlinear APHE, the factor $\tau E^2 B$ is even for both $\mathcal{T}$ and $\mathcal{P}$ symmetry, requiring the WSM Hamiltonian to break both $\mathcal{T}$ and $\mathcal{P}$ symmetry, which is ensured by Eq. (18). Considering the nonlinear APHE is extrinsic, the dependencies on the intranodes and internodes scattering affect the APHE in different ways [67]. It is seen that the nonlinear APHE is mainly dominated by the anisotropy of the distribution function within each valley, which is characterized by the intranode scattering τ. It has been proposed that the chiral anomaly induces nonlinear PHE [61,68,69], in which the current is limited by the internode scattering $\tau_{\rm inter}$, where the quasiparticles scatter across the nodes and switch their chirality. It is therefore implied that the nonlinear APHE manifests in WSMs in the limit when $\tau \gg \tau_{\rm inter}$, where the short-range interaction or short-range scattering dominates over the long-range one [68].

We then solve the second-order APHC tensors induced by E-FBC and B-FBC, which are given by (see Appendix C)

$$\begin{aligned}\sigma^{yxx}_{\rm E\text{-}FBC} = -\frac{e^3\tau}{\hbar}\sum_s\int [d\boldsymbol{k}]\frac{\partial f_0}{\partial\varepsilon_{\boldsymbol{k}}}\frac{1}{2v_F k^5}\big[&v_F k^y R_s^z v_s^y B^x\\ &- v_F k^z R_s^y v_s^y B^x + k^y v_s^z v_s^x B^y\big],\end{aligned} \tag{28}$$

$$\begin{aligned}\sigma^{yxx}_{\rm B\text{-}FBC} = -\frac{e^3\tau}{\hbar}\sum_s\int [d\boldsymbol{k}]\frac{\partial f_0}{\partial\varepsilon_{\boldsymbol{k}}}\frac{v^x}{2k^6}\big[&k^y(2k^z + kR_s^z)B^y\\ &+ k^x(2k^z + kR_s^z)B^x\big].\end{aligned} \tag{29}$$

We consider that a pair of Weyl cones are tilted in the same direction with $\boldsymbol{R}_s = \boldsymbol{R}$. One observes that a finite value of the first term in $\sigma^{yxx}_{\rm E\text{-}FBC}$ requires a nonzero R^z. For the second term in $\sigma^{yxx}_{\rm E\text{-}FBC}$, it is proportional to $k^z(k^y/k + R_s^y)$ that takes a finite value if the tilting vector has both nonzero components along the y and z axes. Similarly, the third term in $\sigma^{yxx}_{\rm E\text{-}FBC}$ takes a finite value if the x, y, and z components of the tilting are nonzero simultaneously. Similar deduction applies to $\sigma^{yxx}_{\rm B\text{-}FBC}$. Recall that a nonvanishing linear FBC-induced APHE requires that the angle (α) between the tilt and the normal of transport plane is not zero, nor $\pi/2$. Thus, when R^z is finite and $R^x = R^y = 0$, the linear APHE vanishes and the second-order APHE dominates, with a second-order APHC (see Appendix C)

$$\sigma^{yxx}_{\rm E\text{-}FBC} = -\frac{e^3\tau}{\hbar}v_{\rm F}\int [d\boldsymbol{k}]\frac{\partial f_0}{\partial\varepsilon_{\boldsymbol{k}}}\frac{(k^y)^2}{k^6}R^z B^x, \tag{30}$$

$$\sigma^{yxx}_{\rm B\text{-}FBC} = -\frac{e^3\tau}{\hbar}v_{\rm F}\int [d\boldsymbol{k}]\frac{\partial f_0}{\partial\varepsilon_{\boldsymbol{k}}}\frac{(k^x)^2}{k^6}R^z B^x. \tag{31}$$

The constraints on the linear and second-order APHCs from the tilting directions are summarized in Table I.

After some algebra, the analytical expressions of Eqs. (30) and (31) are found as (for more details see Appendix D)

$$\sigma^{yxx}_{\rm E\text{-}FBC} = \sigma^{yxx}_{\rm B\text{-}FBC} = -\frac{e^3\tau v_{\rm F}^3\pi}{30\hbar\mu^2}\frac{[5+(R^z)^2]R^z}{\sqrt{1-(R^z)^2}}B^x. \tag{32}$$

As seen in Eq. (32) the nonlinear APHC scales with μ^{-2}, which indicates that the nonlinear APHC increases rapidly when the Fermi level approaches the Weyl nodes. This characteristic is due to the singularity of the quantum metric at the nodes. The FBC-induced nonlinear APHE predicted here vanishes (survives) when the tiling vector lies in (perpendicular to) the transport plane, while the chiral-anomaly induced nonlinear PHE survives (vanishes) [61,65].

VI. CONCLUSIONS AND DISCUSSIONS

In this work we propose a type of APHE originating from the field-induced Berry connection in tilted WSMs, which is closely associated with the quantum metric. As a transport phenomenon, it is distinct from the most remarkable transport phenomena for the WSMs, e.g., the negative longitudinal magnetoresistance and the extrinsic planar Hall effect, which are induced by the chiral anomaly. Due to the intrinsic nature, the APHE proposed here reflects the microscopic geometric properties of Bloch electrons, which could be useful for

band-structure engineering to the observation of the quantum metric by *ab initio* calculations. The FBC-induced nonlinear APHE is also studied. The conditions for the existence of the linear and nonlinear APHE are discussed, revealing that it is possible to distinguish them in experiments.

Note added. Recently, we came across an independent work [70] with a very similar calculation that predicts planar Hall effect related to the field-induced Berry connection. However, their expressions of the planar Hall conductivities are different from ours given in Eqs. (16) and (17). Despite that, it is also found in Ref. [70] that a nonzero requires the tilting is not parallel or perpendicular to the transport plane, as a distinguishable feature of the intrinsic planar Hall effect.

ACKNOWLEDGMENTS

The authors thank Z. F. Zhang for helpful discussions. This work is supported in part by the NSFC (Grants No. 11974348 and No. 11834014), and the National Key R&D Program of China (Grant No. 2018YFA0305800). It is also supported by the Fundamental Research Funds for the Central Universities, and the Strategic Priority Research Program of CAS (Grants No. XDB28000000, and No. XDB33000000). Z.G.Z. is supported in part by the Training Program of Major Research plan of the National Natural Science Foundation of China (Grant No. 92165105), and CAS Project for Young Scientists in Basic Research Grant No. YSBR-057.

APPENDIX A: DERIVATION OF EQS. (21) AND (23)

We can employ spherical coordinates and parametrize the vector $\boldsymbol{k} = k(\sin\theta\cos\phi,\ \sin\theta\sin\phi,\ \cos\theta)$. With the notation $s = 1$ and $\bar{s} = -1$, the eigenstates are

$$|s-\rangle = \begin{pmatrix} \sin(\theta/2)e^{-i\phi} \\ -\cos(\theta/2) \end{pmatrix}, \quad |s+\rangle = \begin{pmatrix} \cos(\theta/2)e^{-i\phi} \\ \sin(\theta/2) \end{pmatrix}. \tag{A1}$$

Making use of the identity $v^{\alpha}_{nm} = -i\varepsilon_{mn}\mathcal{A}^{\alpha}_{nm}$, the intraband Berry connection becomes $\mathcal{A}^{\alpha}_{nm} = i\langle n|\partial^{\alpha}H|m\rangle/(\varepsilon_m - \varepsilon_n)$. By inserting the Hamilton (18) into Eqs. (A2) and (A3), the off-diagonal elements of the quantum metric tensors for the Weyl node with chirality s of the valence band are obtained as

$$\begin{aligned} g^{xy}_{s-} &= \mathrm{Re}\big[\mathcal{A}^{x}_{s-+}\mathcal{A}^{y}_{s+-}\big] = \frac{\mathrm{Re}[\langle s-|\sigma_x|s+\rangle\langle s+|\sigma_y|s-\rangle]n}{(\varepsilon_{s-}-\varepsilon_{s+})^2} \\ &= -\frac{\sin^2(\theta/2)\cos^2(\theta/2)\sin(2\phi)}{2k^2} = -\frac{k_x k_y}{4k^4}. \end{aligned} \tag{A2}$$

And for the conduction band it follows the analogous calculation. It is easy to verity that $g^{\alpha\beta}_{s-} = g^{\beta\alpha}_{s-}$, which testifies the symmetric nature of the quantum metric tensor. The diagonal parts are given by

$$\begin{aligned} & g^{xx}_{s-} \\ &= \mathrm{Re}\big[\mathcal{A}^{x}_{s-+}\mathcal{A}^{x}_{s+-}\big] = \frac{\mathrm{Re}[\langle s-|\sigma_x|s+\rangle\langle s+|\sigma_x|s-\rangle]n}{(\varepsilon_{s-}-\varepsilon_{s+})^2} \\ &= \frac{\sin^4(\theta/2)+\cos^4(\theta/2)-\sin^2(\theta/2)\cos^2(\theta/2)\cos(2\phi)}{4k^2} \\ &= \frac{k_y^2+k_z^2}{4k^4}. \end{aligned} \tag{A3}$$

With the substitution $\boldsymbol{k} \to -\boldsymbol{k}$, we found that $g^{xy}_{s-} = g^{xy}_{\bar{s}-}$. Therefore, one observes that the two cones preserve the same quantum metric, which is distinct from the Berry curvature, since the Berry curvature is opposite for the two cones. According to Eq. (3) in the main text, the E-FBC are given in form of the quantum metric as

$$G^{\alpha\beta}_{s-} = \frac{2g^{\alpha\beta}_{s-}}{\varepsilon_{s-}-\varepsilon_{s+}}. \tag{A4}$$

Making use of the identity $\varepsilon_{s-} - \varepsilon_{s+} = -2v_F k$, it is found that the E-FBC is independent of the chirality and we drop the chiral indices for the E-FBCs in the following. Combining Eqs. (A2), (A3), and (3), the E-FBCs are found as

$$G^{\alpha\beta}_{-} = \frac{k^{\alpha}k^{\beta}}{4v_F k^5}, \quad G^{\alpha\alpha}_{-} = -\frac{k^2-(k^{\alpha})^2}{4v_F k^5}. \tag{A5}$$

For convenience, we introduce the definition

$$\mathcal{G}^{\alpha\beta\gamma} = \partial^{\alpha}G^{\beta\gamma} - \partial^{\beta}G^{\alpha\gamma}. \tag{A6}$$

By use of Eq. (A6), $\sigma^{yx}_{\text{E-FBC}}$ is found as

$$\begin{aligned} \sigma^{yx}_{\text{E-FBC}} = &-\frac{e^2}{\hbar}\sum_s \int [d\boldsymbol{k}]\big(v^x_s\mathcal{G}^{yzx} + v^y_s\mathcal{G}^{zxx} + v^z_s\mathcal{G}^{xyx}\big) \\ &\times f_0 B\sin\theta. \end{aligned} \tag{A7}$$

By placing Eq. (A4) into Eq. (A6), one observes that

$$\begin{aligned} \mathcal{G}^{yzx} &= \partial^z G^{yx} - \partial^y G^{zx} = 0, \\ \mathcal{G}^{zxx} &= -2\frac{k^z}{k^5}, \quad \mathcal{G}^{xyx} = 2\frac{k^y}{k^5}. \end{aligned} \tag{A8}$$

By the use of Eqs. (A5) and (A7), the APHC induced by the E-FBC is obtained as

$$\sigma^{yx}_{\text{E-FBC}} = -\frac{e^2}{\hbar}\int [d\boldsymbol{k}] f_{\text{eq}}\Gamma^{yz}B\sin\theta. \tag{A9}$$

The B-FBC-induced APHC can be obtained similarly. Parallel to Eq. (A6), we introduce the definition

$$\mathcal{F}^{\alpha\beta\gamma}_{s} = \partial^{\alpha}F^{\beta\gamma}_{s} - \partial^{\beta}F^{\alpha\gamma}_{s}. \tag{A10}$$

Plugging Eqs. (A5) and (A10) into Eq. (15), when the pair of Weyl cones are tilted in the same direction the linear APHC induced by the B-FBC is obtained as

$$\sigma^{yx}_{\text{B-FBC}} = \frac{e^2}{\hbar}\int [d\boldsymbol{k}] f_0(\mathcal{F}^{yxy}\sin\theta + \mathcal{F}^{yxx}\cos\theta)B, \tag{A11}$$

with

$$\mathcal{F}^{yxy} = \frac{k^y(2k^z + kR^z)}{2k^6}, \quad \mathcal{F}^{yxx} = \frac{k^x(2k^z + kR^z)}{2k^6}. \tag{A12}$$

APPENDIX B: COMPARISON WITH PLANAR HALL EFFECT INDUCED BY CHIRAL ANOMALY

The chiral-anomaly-induced planar Hall conductivity on the order of $O(EB)$ is given as

$$\sigma^{yx}_{\text{CA}} = -\frac{e^3\tau}{\hbar}\int [d\boldsymbol{k}]B\big(v^y_{\boldsymbol{k}}\cos\theta + v^x_{\boldsymbol{k}}\sin\theta\big)(\boldsymbol{v}_{\boldsymbol{k}}\cdot\boldsymbol{\Omega}_{\boldsymbol{k}}). \tag{B1}$$

As demonstrated in the main text, σ^{yx}_{CA} vanishes when the nodes tilt along the opposite directions, while $\sigma^{yx}_{\text{B-FBC}}$ is finite if

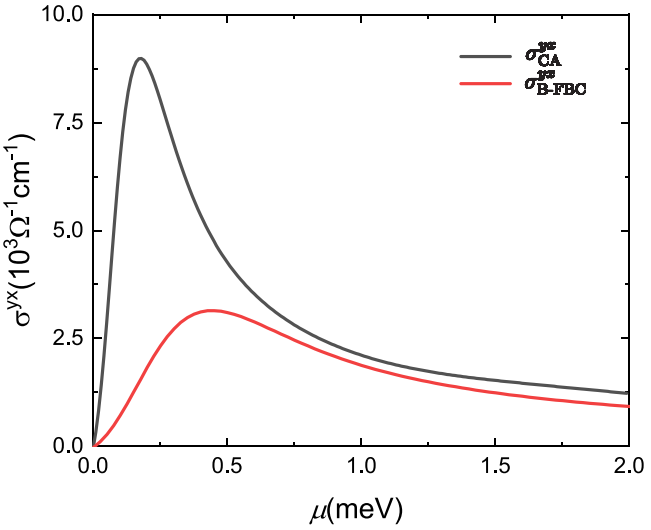

FIG. 2. Planar Hall conductivities induced by the chiral anomaly and the FBC as a function of the chemical potential. The parameters $R^z_s = R^z_{\bar{s}} = 0.25$, $R^y_s = -R^y_{\bar{s}} = 0.25$, $v_F = 2$ eV Å, $B = 0.5$ T, $k_BT = 10$ meV, $\tau = 10^{-13}$ s.

the nodes tilt along the same direction. As a consequence, the PHE induced by the chiral anomaly and the APHE induced by the FBC coexist with a noncollinear tilting. In Fig. 2 we show the comparison between the PHE induced by chiral anomaly and the APHE induced by FBC as a function of the chemical potential, where the tilting of the two nodes is noncollinear. Assuming the relaxation time $\tau = 10^{-13}$ s [61], it can be seen that $\sigma^{yx}_{\text{B-FBC}}$ is on the same order of magnitude of σ^{yx}_{CA}, along with a different peak position versus the chemical potential.

APPENDIX C: DERIVATION OF THE EXPRESSIONS OF THE FBC-INDUCED NONLINEAR APHC IN WEYL SEMIMETALS

From Eq. (25), the second-order APHC tensors induced by E-FBC and B-FBC are obtained as

$$\sigma^{yxx}_{\text{E-FBC}} = \frac{e^3\tau}{\hbar}\int [d\boldsymbol{k}][(\partial^y G^{xx} - \partial^x G^{yx})(B^y v^z - B^z v^y)v^x - (\partial^z G^{yx} - \partial^y G^{zx})(B^x v^y - B^y v^x)v^x + (\partial^x G^{zx} - \partial^z G^{xx})v_y^2 B^x + (\partial^y G^{xx} - \partial^x G^{yx})v^y v^z B^x + (\partial^z G^{yx} - \partial^y G^{zx})v^y v^x B^x]\frac{\partial f_0}{\partial \varepsilon_{\boldsymbol{k}}}, \tag{C1}$$

$$\sigma^{yxx}_{\text{B-FBC}} = -\frac{e^3\tau}{\hbar}\int [d\boldsymbol{k}]\frac{\partial f_0}{\partial \varepsilon_{\boldsymbol{k}}}[\partial^y(F^{xx}B^x + F^{xy}B^y)v^x - \partial^x(F^{yx}B^x + F^{yy}B^y)v^x]. \tag{C2}$$

k space. Making use of the coordinates transformations:

Making use of Eqs. (A6) and (A10), they can be rewritten as

$$\sigma^{yxx}_{\text{E-FBC}} = \frac{e^3\tau}{\hbar}\int [d\boldsymbol{k}][\mathcal{G}^{yxx}(B^y v^z - B^z v^y)v^x - \mathcal{G}^{zyx}(B^x v^y - B^y v^x)v^x + \mathcal{G}^{xzx}(v^y)^2 B^x + \mathcal{G}^{yxx}v^y v^z B^x + \mathcal{G}^{zyx}v^y v^x B^x]\frac{\partial f_0}{\partial \varepsilon_{\boldsymbol{k}}}, \tag{C3}$$

$$\sigma^{yxx}_{\text{B-FBC}} = -\frac{e^3\tau}{\hbar}\int [d\boldsymbol{k}]\frac{\partial f_0}{\partial \varepsilon_{\boldsymbol{k}}}[(\mathcal{F}^{yxy}B^x + \mathcal{F}^{yxx}B^y)v^x - \partial^x(F^{yx}B^x + F^{yy}B^y)v^x]. \tag{C4}$$

Combining with Eqs. (A6) and (A10), we obtain

$$\sigma^{yxx}_{\text{E-FBC}} = -\frac{e^3\tau}{\hbar}\sum_s \int [d\boldsymbol{k}]\frac{\partial f_0}{\partial \varepsilon_{\boldsymbol{k}}}\frac{1}{2v_F k^5} \times \left[v_F k^y R^z_s v^y B^x - v_F k^z R^y_s v^y B^x + k^y v^z_s v^x_s B^y\right], \tag{C5}$$

$$\sigma^{yxx}_{\text{B-FBC}} = -\frac{e^3\tau}{\hbar}\sum_s \int [d\boldsymbol{k}]\frac{\partial f_0}{\partial \varepsilon_{\boldsymbol{k}}}\frac{v^x}{2k^6} \times \left[k^y(2k^z + kR^z_s)B^y + k^x(2k^z + kR^z_s)B^x\right]. \tag{C6}$$

When the pair of Weyl cones are tilted in the same direction, we set R^z finite and R^x and R^y to zero, and the second-order APHC contributed by the E-FBC can be simplified as

$$\sigma^{yxx}_{\text{E-FBC}} = -\frac{e^3\tau}{\hbar}\int [d\boldsymbol{k}]\frac{\partial f_0}{\partial \varepsilon_{\boldsymbol{k}}}v_{\text{F}}\frac{(k^y)^2}{k^6}R^z B^x. \tag{C7}$$

In Eq. (C6) the terms proportional to k^y are nonzero when the tilting vector has both nonzero components along the y and the z axes. The terms proportional to k^x are nonzero when the tilting vector has both nonzero components along the x and the z axes. When R^z is finite and both of R^x and R^y are zero, $\sigma^{yxx}_{\text{B-FBC}}$ is written as

$$\sigma^{yxx}_{\text{B-FBC}} = -\frac{e^3\tau}{\hbar}\int [d\boldsymbol{k}]\frac{\partial f_0}{\partial \varepsilon_{\boldsymbol{k}}}v_{\text{F}}\frac{(k^x)^2}{k^6}R^z B^x. \tag{C8}$$

APPENDIX D: DERIVATION OF THE ANALYTICAL FORM OF SECOND-ORDER APHC

To obtain the analytic formulas of the nonlinear APHC tensors, one needs to deal with the integrals in Eqs. (30) and (31) in the main text. According to Eq. (30), the E-FBC-induced second-order magnetoconductivity is written as

$$\sigma^{yxx}_{\text{E-FBC}} = -\frac{e^3\tau}{\hbar}v_{\text{F}}\int [d\boldsymbol{k}]\frac{\partial f^0}{\partial \varepsilon_{\boldsymbol{k}}}\frac{(k^y)^2}{2k^6}R^z B^x. \tag{D1}$$

Let us suppose that the Fermi energy lies above the Weyl points, namely, $\mu > 0$, so that only the conduction band is considered. To derive an analytical expression, we consider the zero-temperature limit, so that the partial derivative of the Fermi-Dirac distribution is a δ function, $\partial f_0/\partial\varepsilon = \delta(\varepsilon - \mu)$. Owing to the tilting, the equi-energy surfaces are ellipsoid in

$$k^{x\prime} = k^x,\ k^{y\prime} = k^y,\ k^{z\prime} = \sqrt{1-(R^z)^2}\left(k^z + \frac{\varepsilon}{v_F}\frac{R^z}{1-(R^z)^2}\right), \tag{D2}$$

where $k' = [(k^{x\prime})^2 + (k^{y\prime})^2 + (k^{z\prime})^2]^{1/2}$, and the integral element is changed as $\int [d\boldsymbol{k}] \to \int [d\boldsymbol{k}'][1-(R^z)^2]^{-1/2}$. The partial derivative becomes $\partial f/\partial\varepsilon = \delta(\mu - v_F k'[1-(R^z)^2]^{1/2})$:

$$\begin{aligned}\sigma^{yxx}_{\text{E-FBC}} &= -\frac{e^3\tau}{\hbar} v_{\text{F}} \int [d\boldsymbol{k}'] \frac{R^z}{\sqrt{1-(R^z)^2}} \frac{(k^{y\prime})^2}{2\Big[\sqrt{1-(R^z)^2}k' - R^z\Big(\frac{1}{\sqrt{1-(R^z)^2}}k^{z\prime} - \frac{\varepsilon}{v_F}\frac{R^z}{1-(R^z)^2}\Big)\Big]^6} \delta(\mu - v_F k'\sqrt{1-(R^z)^2}) B^x \\ &= -\frac{e^3\tau}{\hbar} v_{\text{F}} \int_0^{2\pi} d\phi \int_0^{\pi} d\theta \frac{R^z}{\sqrt{1-(R^z)^2}} \left(\frac{\sqrt{1-(R^z)^2}}{R^z k'}\right)^6 \frac{k'^4 \sin\theta^3 \cos\phi^2}{\big(\frac{1}{R^z} - \cos\theta\big)^6} \delta(\mu - v_F k'\sqrt{1-(R^z)^2}) B^x \\ &= -\frac{e^3\tau v_{\text{F}}^3 \pi}{30\hbar\mu^2} \frac{[5+(R^z)^2]R^z}{\sqrt{1-(R^z)^2}} B^x, \end{aligned} \tag{D3}$$

where the integral is calculated in spherical coordinates with

$$k'_x = k'\sin\theta\cos\phi, \quad k'_y = k'\sin\theta\sin\phi, \quad k'_z = k'\cos\theta. \tag{D4}$$

In a similar manner, the B-FBC contribution to the nonlinear APHE is obtained as

$$\sigma^{yxx}_{\text{B-FBC}} = -\frac{e^3\tau v_{\text{F}}^3 \pi}{30\hbar\mu^2} \frac{[5+(R^z)^2]R^z}{\sqrt{1-(R^z)^2}} B^x, \tag{D5}$$

[1] X. Wan, A. M. Turner, A. Vishwanath, and S. Y. Savrasov, Topological semimetal and Fermi-arc surface states in the electronic structure of pyrochlore iridates, Phys. Rev. B **83**, 205101 (2011).

[2] H. Weng, C. Fang, Z. Fang, B. A. Bernevig, and X. Dai, Weyl semimetal phase in noncentrosymmetric transition-metal monophosphides, Phys. Rev. X **5**, 011029 (2015).

[3] B. Q. Lv, H. M. Weng, B. B. Fu, X. P. Wang, H. Miao, J. Ma, P. Richard, X. C. Huang, L. X. Zhao, G. F. Chen, Z. Fang, X. Dai, T. Qian, and H. Ding, Experimental discovery of Weyl semimetal TaAs, Phys. Rev. X **5**, 031013 (2015).

[4] S.-Y. Xu, I. Belopolski, N. Alidoust, M. Neupane, G. Bian, C. Zhang, R. Sankar, G. Chang, Z. Yuan, C.-C. Lee, S.-M. Huang, H. Zheng, J. Ma, D. S. Sanchez, B. Wang, A. Bansil, F. Chou, P. P. Shibayev, H. Lin, S. Jia *et al.*, Discovery of a Weyl fermion semimetal and topological Fermi arcs, Science **349**, 613 (2015).

[5] S.-Y. Xu, I. Belopolski, D. S. Sanchez, C. Zhang, G. Chang, C. Guo, G. Bian, Z. Yuan, H. Lu, T.-R. Chang, P. P. Shibayev, M. L. Prokopovych, N. Alidoust, H. Zheng, C.-C. Lee, S.-M. Huang, R. Sankar, F. Chou, C.-H. Hsu, H.-T. Jeng *et al.*, Experimental discovery of a topological Weyl semimetal state in tap, Sci. Adv. **1**, e1501092 (2015).

[6] M. Z. Hasan, S.-Y. Xu, I. Belopolski, and S.-M. Huang, Discovery of Weyl fermion semimetals and topological Fermi arc states, Annu. Rev. Condens. Matter Phys. **8**, 289 (2017).

[7] B. Yan and C. Felser, Topological materials: Weyl semimetals, Annu. Rev. Condens. Matter Phys. **8**, 337 (2017).

[8] N. P. Armitage, E. J. Mele, and A. Vishwanath, Weyl and Dirac semimetals in three-dimensional solids, Rev. Mod. Phys. **90**, 015001 (2018).

[9] K.-Y. Yang, Y.-M. Lu, and Y. Ran, Quantum Hall effects in a Weyl semimetal: Possible application in pyrochlore iridates, Phys. Rev. B **84**, 075129 (2011).

[10] A. A. Burkov and L. Balents, Weyl semimetal in a topological insulator multilayer, Phys. Rev. Lett. **107**, 127205 (2011).

[11] G. Xu, H. Weng, Z. Wang, X. Dai, and Z. Fang, Chern semimetal and the quantized anomalous Hall effect in $HgCr_2Se_4$, Phys. Rev. Lett. **107**, 186806 (2011).

[12] W. Jiang, D. J. P. de Sousa, J.-P. Wang, and T. Low, Giant anomalous Hall effect due to double-degenerate quasiflat bands, Phys. Rev. Lett. **126**, 106601 (2021).

[13] D. T. Son and B. Z. Spivak, Chiral anomaly and classical negative magnetoresistance of Weyl metals, Phys. Rev. B **88**, 104412 (2013).

[14] A. A. Burkov, Chiral anomaly and diffusive magnetotransport in Weyl metals, Phys. Rev. Lett. **113**, 247203 (2014).

[15] D. E. Kharzeev and H.-U. Yee, Anomaly induced chiral magnetic current in a Weyl semimetal: Chiral electronics, Phys. Rev. B **88**, 115119 (2013).

[16] S. A. Parameswaran, T. Grover, D. A. Abanin, D. A. Pesin, and A. Vishwanath, Probing the chiral anomaly with nonlocal transport in three-dimensional topological semimetals, Phys. Rev. X **4**, 031035 (2014).

[17] A. A. Burkov, Chiral anomaly and transport in Weyl metals, J. Phys.: Condens. Matter **27**, 113201 (2015).

[18] V. A. Zyuzin, Magnetotransport of Weyl semimetals due to the chiral anomaly, Phys. Rev. B **95**, 245128 (2017).

[19] K.-S. Kim, H.-J. Kim, and M. Sasaki, Boltzmann equation approach to anomalous transport in a Weyl metal, Phys. Rev. B **89**, 195137 (2014).

[20] S. Nandy, G. Sharma, A. Taraphder, and S. Tewari, Chiral anomaly as the origin of the planar Hall effect in Weyl semimetals, Phys. Rev. Lett. **119**, 176804 (2017).

[21] A. A. Burkov, Giant planar Hall effect in topological metals, Phys. Rev. B **96**, 041110(R) (2017).

[22] S. Ghosh, D. Sinha, S. Nandy, and A. Taraphder, Chirality-dependent planar Hall effect in inhomogeneous Weyl semimetals, Phys. Rev. B **102**, 121105(R) (2020).

[23] D. T. Son and N. Yamamoto, Berry curvature, triangle anomalies, and the chiral magnetic effect in Fermi liquids, Phys. Rev. Lett. **109**, 181602 (2012).

[24] M. A. Stephanov and Y. Yin, Chiral kinetic theory, Phys. Rev. Lett. **109**, 162001 (2012).

[25] K. Landsteiner, E. Megías, and F. Pena-Benitez, Gravitational anomaly and transport phenomena, Phys. Rev. Lett. **107**, 021601 (2011).

[26] M.-C. Chang and M.-F. Yang, Chiral magnetic effect in a two-band lattice model of Weyl semimetal, Phys. Rev. B **91**, 115203 (2015).

[27] R. Battilomo, N. Scopigno, and C. Ortix, Anomalous planar Hall effect in two-dimensional trigonal crystals, Phys. Rev. Res. **3**, L012006 (2021).

[28] T. Kurumaji, Symmetry-based requirement for the measurement of electrical and thermal Hall conductivity under an in-plane magnetic field, Phys. Rev. Res. **5**, 023138 (2023).

[29] M. V. Berry, Quantal phase factors accompanying adiabatic changes, Proc. R. Soc. London, Ser. A **392**, 45 (1984).

[30] A. Shapere and F. Wilczek, *Geometric Phases in Physics* (World Scientific, Singapore, 1989), Vol. 5.

[31] J. Provost and G. Vallee, Riemannian structure on manifolds of quantum states, Commun. Math. Phys. **76**, 289 (1980).

[32] V. Bužek and M. Hillery, Quantum copying: Beyond the no-cloning theorem, Phys. Rev. A **54**, 1844 (1996).

[33] V. Vedral, M. B. Plenio, M. A. Rippin, and P. L. Knight, Quantifying entanglement, Phys. Rev. Lett. **78**, 2275 (1997).

[34] T. Baumgratz, M. Cramer, and M. B. Plenio, Quantifying coherence, Phys. Rev. Lett. **113**, 140401 (2014).

[35] K. Życzkowski and H.-J. Sommers, Average fidelity between random quantum states, Phys. Rev. A **71**, 032313 (2005).

[36] D. Leibfried, B. DeMarco, V. Meyer, D. Lucas, M. Barrett, J. Britton, W. M. Itano, B. Jelenković, C. Langer, T. Rosenband *et al.*, Experimental demonstration of a robust, high-fidelity geometric two ion-qubit phase gate, Nature (London) **422**, 412 (2003).

[37] S. Peotta and P. Törmä, Superfluidity in topologically nontrivial flat bands, Nat. Commun. **6**, 8944 (2015).

[38] A. Julku, S. Peotta, T. I. Vanhala, D.-H. Kim, and P. Törmä, Geometric origin of superfluidity in the Lieb-lattice flat band, Phys. Rev. Lett. **117**, 045303 (2016).

[39] O. Bleu, G. Malpuech, Y. Gao, and D. D. Solnyshkov, Effective theory of nonadiabatic quantum evolution based on the quantum geometric tensor, Phys. Rev. Lett. **121**, 020401 (2018).

[40] Y. Gao and D. Xiao, Nonreciprocal directional dichroism induced by the quantum metric dipole, Phys. Rev. Lett. **122**, 227402 (2019).

[41] P. Törmä, S. Peotta, and B. A. Bernevig, Superconductivity, superfluidity and quantum geometry in twisted multilayer systems, Nat. Rev. Phys. **4**, 528 (2022).

[42] Y. Gao, S. A. Yang, and Q. Niu, Field induced positional shift of Bloch electrons and its dynamical implications, Phys. Rev. Lett. **112**, 166601 (2014).

[43] Y. Gao, S. A. Yang, and Q. Niu, Geometrical effects in orbital magnetic susceptibility, Phys. Rev. B **91**, 214405 (2015).

[44] V. A. Zyuzin, In-plane Hall effect in two-dimensional helical electron systems, Phys. Rev. B **102**, 241105(R) (2020).

[45] H. Wang, Y.-X. Huang, H. Liu, X. Feng, J. Zhu, W. Wu, C. Xiao, and S. A. Yang, Theory of intrinsic in-plane Hall effect, arXiv:2211.05978.

[46] S. S. Tsirkin and I. Souza, On the separation of Hall and Ohmic nonlinear responses, SciPost Phys. Core **5**, 039 (2022).

[47] Y. Gao, Semiclassical dynamics and nonlinear charge current, Front. Phys. **14**, 33404 (2019).

[48] H. Liu, J. Zhao, Y.-X. Huang, W. Wu, X.-L. Sheng, C. Xiao, and S. A. Yang, Intrinsic second-order anomalous Hall effect and its application in compensated antiferromagnets, Phys. Rev. Lett. **127**, 277202 (2021).

[49] E. Rossi, Quantum metric and correlated states in two-dimensional systems, Curr. Opin. Solid State Mater. Sci. **25**, 100952 (2021).

[50] T. Holder, D. Kaplan, and B. Yan, Consequences of time-reversal-symmetry breaking in the light-matter interaction: Berry curvature, quantum metric, and diabatic motion, Phys. Rev. Res. **2**, 033100 (2020).

[51] D. Xiao, M.-C. Chang, and Q. Niu, Berry phase effects on electronic properties, Rev. Mod. Phys. **82**, 1959 (2010).

[52] C. Duval, Z. Horváth, P. A. Horvathy, L. Martina, and P. Stichel, Berry phase correction to electron density in solids and "exotic" dynamics, Mod. Phys. Lett. B **20**, 373 (2006).

[53] D. Xiao, J. Shi, and Q. Niu, Berry phase correction to electron density of states in solids, Phys. Rev. Lett. **95**, 137204 (2005).

[54] K. Das and A. Agarwal, Intrinsic Hall conductivities induced by the orbital magnetic moment, Phys. Rev. B **103**, 125432 (2021).

[55] D. Ma, H. Jiang, H. Liu, and X. C. Xie, Planar Hall effect in tilted Weyl semimetals, Phys. Rev. B **99**, 115121 (2019).

[56] D. N. Page, Geometrical description of Berry's phase, Phys. Rev. A **36**, 3479 (1987).

[57] I. Bengtsson and K. Życzkowski, *Geometry of Quantum States: An Introduction to Quantum Entanglement* (Cambridge University Press, Cambridge, England, 2017).

[58] R. Cheng, Quantum geometric tensor (Fubini-study metric) in simple quantum system: A pedagogical introduction, arXiv:1012.1337.

[59] J. Ge, D. Ma, Y. Liu, H. Wang, Y. Li, J. Luo, T. Luo, Y. Xing, J. Yan, D. Mandrus, H. Liu, X. C. Xie, and J. Wang, Unconventional Hall effect induced by Berry curvature, Natl. Sci. Rev. **7**, 1879 (2020).

[60] F. Arnold, M. Naumann, S.-C. Wu, Y. Sun, M. Schmidt, H. Borrmann, C. Felser, B. Yan, and E. Hassinger, Chiral Weyl pockets and Fermi surface topology of the Weyl semimetal TaAs, Phys. Rev. Lett. **117**, 146401 (2016).

[61] R.-H. Li, O. G. Heinonen, A. A. Burkov, and S. S.-L. Zhang, Nonlinear Hall effect in Weyl semimetals induced by chiral anomaly, Phys. Rev. B **103**, 045105 (2021).

[62] Y. Zhang, Y. Sun, and B. Yan, Berry curvature dipole in Weyl semimetal materials: An *ab initio* study, Phys. Rev. B **97**, 041101(R) (2018).

[63] C. Zeng, S. Nandy, and S. Tewari, Nonlinear transport in Weyl semimetals induced by Berry curvature dipole, Phys. Rev. B **103**, 245119 (2021).

[64] O. Matsyshyn and I. Sodemann, Nonlinear Hall acceleration and the quantum rectification sum rule, Phys. Rev. Lett. **123**, 246602 (2019).

[65] S. Nandy, C. Zeng, and S. Tewari, Chiral anomaly induced nonlinear Hall effect in semimetals with multiple Weyl points, Phys. Rev. B **104**, 205124 (2021).

[66] Y.-X. Huang, X. Feng, H. Wang, C. Xiao, and S. A. Yang, Intrinsic nonlinear planar Hall effect, Phys. Rev. Lett. **130**, 126303 (2023).

[67] G. Sharma, S. Nandy, K. V. Raman, and S. Tewari, Decoupling intranode and internode scattering in Weyl fermions, Phys. Rev. B **107**, 115161 (2023).

[68] T. Morimoto and N. Nagaosa, Chiral anomaly and giant magnetochiral anisotropy in noncentrosymmetric Weyl semimetals, Phys. Rev. Lett. **117**, 146603 (2016).

[69] D. Mandal, K. Das, and A. Agarwal, Chiral anomaly and nonlinear magnetotransport in time reversal symmetric Weyl semimetals, Phys. Rev. B **106**, 035423 (2022).

[70] L. Xiang and J. Wang, Intrinsic planar Hall effect in tilted Weyl semimetals, arXiv:2209.03527.